Catalysis at a dinuclear [CuSMo(=O)OH] cluster in a CO dehydrogenase resolved at 1.1-Å resolution

Holger Dobbek*†‡, Lothar Gremer†§, Reiner Kiefersauer*¶, Robert Huber*, and Ortwin Meyer‡§‖

*Abteilung Strukturforschung, Max-Planck-Institut für Biochemie, and ¶Proteros Biostructures GmbH, D-82152 Martinsried, Germany; and §Lehrstuhl für Mikrobiologie and ‖Bayreuther Zentrum für Molekulare Biowissenschaften, Universität Bayreuth, D-95440 Bayreuth, Germany

Contributed by Robert Huber, October 22, 2002

The CO dehydrogenase of the eubacterium *Oligotropha carboxidovorans* is a 277-kDa Mo- and Cu-containing iron-sulfur flavoprotein. Here, the enzyme's active site in the oxidized or reduced state, after inactivation with potassium cyanide or with n-butylisocyanide bound to the active site, has been reinvestigated by multiple wavelength anomalous dispersion measurements at atomic resolution, electron spin resonance spectroscopy, and chemical analyses. We present evidence for a dinuclear heterometal [CuSMo(=O)OH] cluster in the active site of the oxidized or reduced enzyme, which is prone to cyanolysis. The cluster is coordinated through interactions of the Mo with the dithiolate pyran ring of molybdopterin cytosine dinucleotide and of the Cu with the Sγ of Cys-388, which is part of the active-site loop VAYRC^{388}SFR. The previously reported active-site structure [Dobbek, H., Gremer, L., Meyer, O. & Huber, R. (1999) *Proc. Natl. Acad. Sci. USA* 96, 8884–8889] of an Mo with three oxygen ligands and an SeH-group bound to the Sγ atom of Cys-388 could not be confirmed. The structure of CO dehydrogenase with the inhibitor n-butylisocyanide bound has led to a model for the catalytic mechanism of CO oxidation which involves a thiocarbonate-like intermediate state. The dinuclear [CuSMo(=O)OH] cluster of CO dehydrogenase establishes a previously uncharacterized class of dinuclear molybdoenzymes containing the pterin cofactor.

Carbon monoxide dehydrogenases (CODHs) of aerobic or anaerobic Bacteria and Archaea, which represent the essential catalyst in the global biogeochemical cycle of atmospheric carbon monoxide (CO), catalyze the oxidation of CO to carbon dioxide (CO_2) or the reverse reaction [$CO + H_2O \leftrightarrow CO_2 + 2\ H^+ + 2\ e^-$] (1, 2). The annual removal of CO from the lower atmosphere and earth by microorganisms has been estimated to be $\approx 1 \times 10^8$ tons (3). Thus, an important role of CODHs is to remove CO from the environment, helping to maintain the toxic gas at subhazardous concentrations.

The Ni-containing CODHs from the anaerobic hydrogenogenic bacteria *Carboxydothermus hydrogenoformans* (4, 5) or *Rhodospirillum rubrum* (6) and the Mo-containing CODHs from the aerobic carboxidotrophic bacteria *Oligotropha carboxidovorans* (7–9) or *Hydrogenophaga pseudoflava* (10) have been structurally characterized. The homodimeric CODHs of *C. hydrogenoformans* or *R. rubrum* contain five metal clusters, of which clusters B, B′ and a subunit-bridging, surface-exposed cluster D are cubane-type [4Fe-4S] clusters (5, 6). The active-site clusters C and C′ of the *C. hydrogenoformans* CODH are asymmetric [Ni-4Fe-5S] clusters identified in the enzyme reduced with dithionite. Their integral Ni ion, which is the likely site of CO oxidation, is coordinated by four sulfur ligands with square planar geometry (5). Interestingly, the corresponding cluster of the CODH from *R. rubrum* has been described as an Fe mononuclear site in combination with an [$NiFe_3S_4$] cubane (6).

CODH from *O. carboxidovorans* consists of a dimer of LMS heterotrimers (7). Each heterotrimer is composed of a 17.8-kDa iron-sulfur protein (S), which carries two types of [2Fe-2S] clusters, a 30.2-kDa flavoprotein (M), which contains a noncovalently bound FAD cofactor, and an 88.7-kDa molybdoprotein (L), which harbors the active site of the enzyme. In a previous paper (7), a CODH preparation with a specific activity of 6.6 units/mg was analyzed at a resolution of 2.2 Å. The enzyme's active site was modeled to contain Mo with three oxygen ligands, the molybdopterin cytosine dinucleotide (MCD) cofactor, and an SeH-group bound to the Sγ atom of Cys-388. In the present paper, we have applied multiple wavelength anomalous dispersion methods at up to 1.09-Å resolution to crystals containing fully functional CODH (23.2 units/mg). The SeH-group could not be confirmed, and a Cu atom was identified instead, at the position formerly assigned to Se. In addition, one of the previously modeled oxygen ligands at the Mo is in the active enzyme μ-sulfido ligand which bridges the metals, thereby forming a dinuclear heterometal [CuSMo(=O)OH] cluster. This interpretation is in accordance with a [$CuSMo(=O)_2$] cluster which has been characterized in the same enzyme by x-ray absorption spectroscopy (XAS; ref. 11). Both the μ-sulfido ligand and the Cu are cyanolysable because they react with cyanide, yielding thiocyanate (SCN^-) and, most likely, copper cyanide (CuCN). Geometry and reactivity of the bimetallic cluster have been studied in crystals of CODH at different catalytic states (oxidized, reduced, reacted with cyanide or n-butylisocyanide) at near or true atomic resolution.

Materials and Methods

CODH from *O. carboxidovorans* was isolated, purified, and crystallized as described (7, 9). Enzymatic oxidation of CO was followed photometrically with 1-phenyl-2-(4-iodophenyl)-3-(4-nitrophenyl)-2*H*-tetrazolium chloride (INT)/1-methoxyphenazine methosulfate (MPMS) as artificial electron acceptors (12). One unit is defined as 1 μmol of CO oxidized per min at 303 K.

[^{75}Se]-labeled CODH was purified from bacteria cultivated with CO in mineral medium (200-ml culture volumes) containing 1.18 μM sodium selenite and supplemented with 46.3 nCi/ml (1 Ci = 37 GBq) [^{75}Se]sodium selenite. SDS/PAGE and autoradiography were used to study the distribution of the label in the three enzyme polypeptides.

Metal analysis by inductively coupled plasma atomic emission spectroscopy (ICP-AES) was performed on an Integra XMP spectrometer (GPC Scientific Equipment, Dundenong, Australia).

Electron spin resonance (epr) spectra were recorded on a Bruker EMX 6-1 spectrometer (Rheinstetten, Germany) equipped with an He-cryostat (Oxford Instruments, Oxon, U.K.), as detailed (9).

Wet ashing of CODH for Cu epr analysis was performed as follows: CODH (0.6 ml, 10.8 μM in 50 mM Hepes buffer, pH 7.2) was supplied with 0.15 ml of 96% (vol/vol) sulfuric acid, incubated for 2 h at 453 K, and residual organic material was oxidized by adding a few drops of 30% (vol/vol) aqueous

Abbreviations: CO, carbon monoxide; CODH, CO dehydrogenase; epr, electron spin resonance.

Data deposition: The atomic coordinates have been deposited in the Protein Data Bank, www.rcsb.org (PDB ID codes 1N5W and 1N60–1N63).

†H.D. and L.G. contributed equally to this work.

‡To whom correspondence may be addressed. E-mail: dobbek@biochem.mpg.de or ortwin.meyer@uni-bayreuth.de.

BIOCHEMISTRY

Table 1. Data and refinement statistics

Data set	Total/unique reflections	R_s*	Resolution, Å	Completeness, %	I/σI, overall/ last shell	Model *R*/ R_{free}-factor, % (last shell)†	Resolution, Å	rms bond, Å	rms angle, °
Ox-sync	941420/387014	0.046	1.49	95.9	25.1/3.5	13.5/16.9 (13/20)	18-1.5	0.017	1.946
Ox-rota	717598/212719	0.087	1.85	99.0	6.0/1.8	18.5/21.1	20.0-1.85	0.007	1.40
Dithio	2011470/632876	0.066	1.28	98.9	22.5/1.9	14.8/18.0 (19/24)	17-1.3	0.019	1.747
nBIC	3044532/931603	0.081	1.09	94.5	19.1/2.0	14.4/17.3 (24/32)	17.8-1.09	0.019	1.892
CN	2299197/744094	0.077	1.19	95.6	20.8/2.1	14.2/17.2 (23/28)	17.8-1.19	0.020	2.00
CO-red	2234419/707024	0.073	1.21	94.1	25.2/1.9	14.9/18.5 (21/25)	17.0-1.21	0.019	1.916
H_2-red	487036/147689	0.111	2.10	97.8	4.6/2.4	18.4/21.0	18.0-2.1	0.012	1.64

Ox-sync, oxidized CODH crystal measured at the synchrotron; Ox-rota, oxidized CODH crystal measured on a rotating Cu-anode x-ray generator; Dithio, dithionite-reduced CODH crystal measured at the synchrotron; nBIC, n-butylisocyanide-soaked CODH crystal measured at the synchrotron; CN, cyanide-soaked CODH crystal measured at the synchrotron; CO-red, CO-reduced CODH crystal measured at the synchrotron; H_2-red, H_2-reduced CODH crystal measured on a rotating Cu-anode x-ray generator.

*$R_s = \Sigma(I - \langle I \rangle)/\Sigma(I)$; measured intensity, $\langle I \rangle$ averaged value; the summation is over all measurements.

†The free R-factor was calculated from 1% of the data for dataset Ox, Dithio, nBIC, CN, and CO-red and 5% for datasets H_2-red and Ox-rota, which were removed at random before the refinement was carried out.

hydrogen peroxide under heating until a translucent assay was obtained. Final sample volumes of 0.3 ml were adjusted with water.

The effect of the oxidation state of CODH on the inactivation with n-butylisocyanide was studied as follows: CODH (5.04 μM in 50 mM Hepes buffer, pH 7.2, kept under an atmosphere of pure Ar) was reduced either by adding 5 mM of sodium dithionite or by flushing with pure CO for 5 min. Assays were adjusted to 1 mM n-butylisocyanide, and the time courses of specific CODH activities were recorded after injection of 5 μl of CODH to the INT/MPMS assay (12).

The effect of n-butylisocyanide, n-butylcyanide, or n-butanol on the specific activity of oxidized CODH was studied by adding 0.1 μM to 10 mM of the indicated compounds to the INT/MPMS assay (12). Then, 5 μl of oxidized CODH (5.04 μM in 50 mM Hepes buffer, pH 7.2) were injected into 1 ml of the test mix (12) and preincubated for 4 min at 303 K. Reactions were started by injection of 0.2 ml of buffer saturated with CO.

Crystal transformation by controlled changes of humidity on a free mounting system at 294 K (13) was applied to optimize the diffraction quality of CODH crystals obtained, as reported (7).

Crystallized CODH was either reduced under anoxic conditions by supplying the carrier gas used for crystal transformation with CO (10% CO in N_2) or H_2 (5% H_2 in N_2) or by the addition of 10 mM sodium dithionite in the harvesting buffer followed by transformation in a stream of pure N_2. After reaching their optimal diffraction quality in the humid crystal-preserving carrier gas-stream, the crystals were shock-frozen by applying a separate stream of N_2 at 100 K and stored in liquid N_2. Crystals were measured by using either a rotating Cu-anode x-ray generator (RTP 300-RC, Rigaku, Tokyo) or synchrotron radiation (BW6, Deutsches Elektronen Synchrotron, Hamburg, Germany).

Not transformed CODH crystals diffracted at the synchrotron to 2.2-Å resolution (7), whereas transformed crystals diffracted to 1.1–1.3 Å. To minimize photoreduction of the metal centers, a dataset of a frozen oxidized crystal was collected in <1 h at the synchrotron to 1.48-Å resolution. The Cu-Mo distance was used as an indicator for photoreduction of the oxidized crystal through intense synchrotron radiation, because the position of heavy scatterers can be determined accurately by crystallography and extended x-ray absorption fine structure (EXAFS), and the distance between the metals depends strongly on the oxidation state of Mo. The Mo…Cu distance of 3.74 Å is in good agreement with EXAFS studies on air-oxidized CODH (Mo…Cu, 3.70 Å; ref. 11) and a high resolution structure (Table 1, dataset Ox-rota) of an oxidized crystal measured on a rotating Cu-anode x-ray generator (Mo…Cu, 3.7 Å).

The structures were refined with SHELX (14) and REFMAC (15) by using the capability of the programs to refine anisotropic displacement parameters and to handle disordered regions. Model building was done with XTALVIEW (16) and MAIN (17).

Results

Description of the CODH-Preparation Used. *O. carboxidovorans* naturally contains functional CODH along with nonfunctional forms which are likely precursors in the posttranslational assembly of the bimetallic cluster in the enzyme's active site (11). The functional and nonfunctional species of CODH copurify because of the same quaternary structure. The preparation of CODH investigated in the previous paper (7) had a specific activity of 6.6 units/mg, indicating a high proportion of nonfunctional enzyme species. The CODH used here had a specific activity of 23.2 units/mg (k_{cat} of 107 s^{-1}).

The degree of catalytic competence of the CODH active site is indicated by how far the iron-sulfur centers (maximum absorption at 550 nm) and the FAD cofactor (maximum absorption at 460 nm) are reduced upon exposure of CODH to CO relative to the reduction with dithionite. In the functional enzyme, CO completely reduces the iron-sulfur centers and the FAD cofactor, which can be followed by UV/visible absorption spectroscopy (Fig. 1*AI*). In nonfunctional CODH, these cofactors remain oxidized. The cofactors are reduced by dithionite irrespective of whether CODH is functional or nonfunctional. Upon exposure to CO, the absorbances of CODH (23.2 units/mg) at 460 or 550 nm (Fig. 1*AI*, traces a and b) decreased by 94 ± 2% ($n = 4$) in comparison to the dithionite-reduced enzyme (Fig. 1*AII*, traces a and b). In addition, the redox difference spectra of CODH reduced with CO or dithionite (Fig. 1*A I* and *II* trace c) are the same. These data represent 6% of nonfunctional enzyme species in the CODH preparation studied in this paper.

A Cu-Ion Occupies the Position in the Active Site Where Formerly an SeH-Group Had Been Modeled. Analyses of functional CODH by neutron activation (Se, Ni) or ICP-AES (all other elements) revealed (mol of metal per mol of enzyme) 7.92 ± 0.18 Fe, 1.96 ± 0.08 Cu, 1.88 ± 0.09 Mo, 1.02 ± 0.06 Se, <0.15 Zn, and <0.05 Ni. Although Cu had been identified long before in CODH (18), the element was subsequently not considered an integral constituent of the enzyme because of the observations that low concentrations of $CuCl_2$ abolished CODH activity (18), epr spectra showed no Cu^{II} signal (Fig. 1 *B* and *C*, trace a), and visible absorption spectra did not show the absorption band

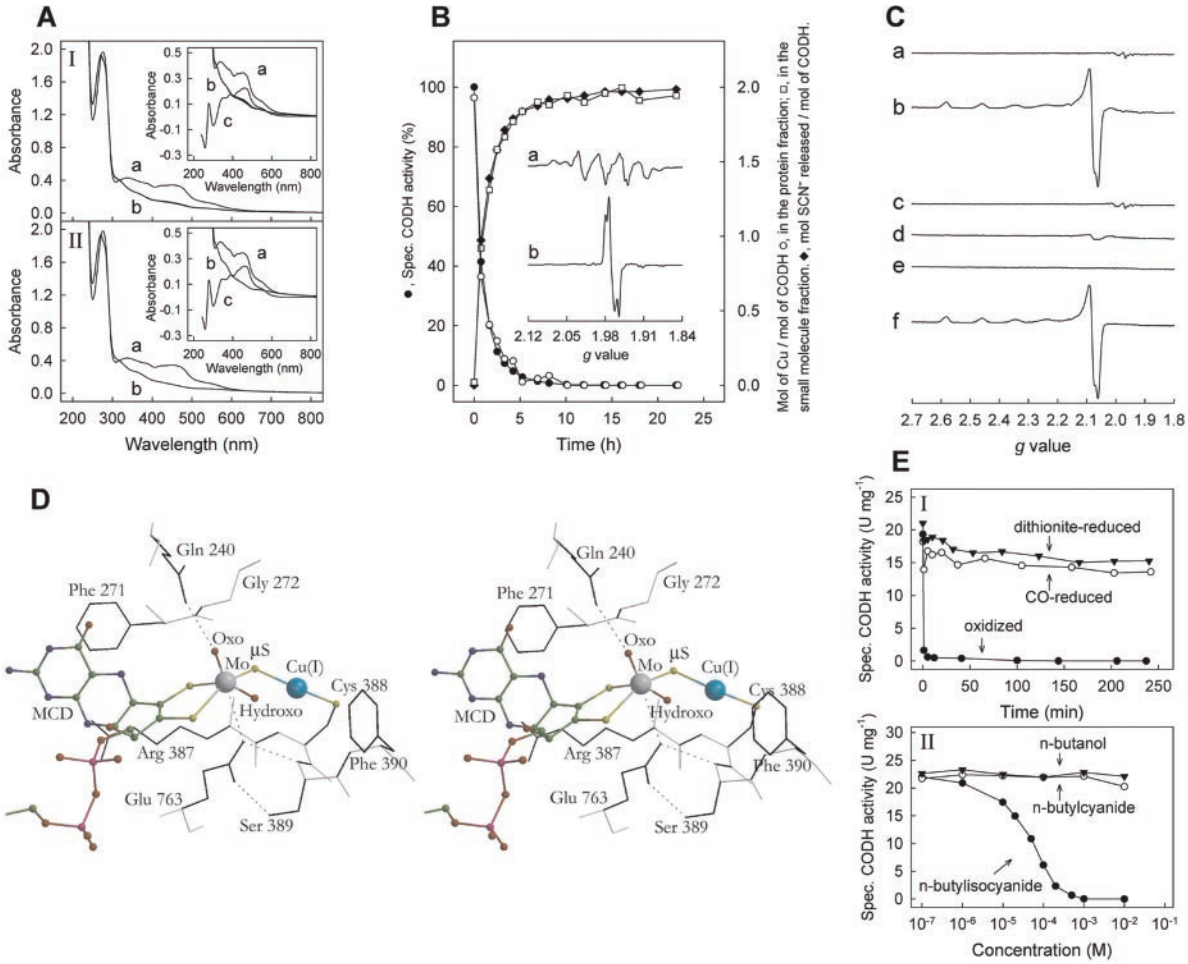

Fig. 1. (*A*) UV/visible spectra of CODH after reduction with CO (*I*) or dithionite (*II*). (*I*) Curve a, air-oxidized; curve b, reduced with pure CO for 1, 15, 30, or 60 min, respectively. (*Inset c*) Difference spectrum of air-oxidized minus CO-reduced for 60 min. (*II*) Curve a, air-oxidized; curve b, reduced with 325 μM dithionite under an atmosphere of pure Ar for 4 min. The spectrum has been corrected with respect to the absorbance of unreacted dithionite. (*Inset c*) Difference spectrum of air-oxidized minus dithionite-reduced. CODH (4.8 μM) was in 50 mM Hepes buffer, pH 7.2. (*B*) Reactivity of CODH with potassium cyanide. CODH (10.8 μM in 50 mM Hepes buffer, pH 7.2; specific activity of 23.2 units/mg, set at 100%) was incubated with 5 mM potassium cyanide under an atmosphere of pure Ar. Samples were fractionated by ultrafiltration (30-kDa cutoff) into the protein fraction and the small molecule fraction. Cu was analyzed in both fractions by inductively coupled plasma atomic emission spectroscopy. Thiocyanate in the small molecule fraction was analyzed colorimetrically as $Fe(SCN)_3$ (31). The specific CO-oxidizing activities were determined in the protein fraction. (*Inset*) Epr spectra of CODH (36 μM) before (a) and after (b) inactivation with 5 mM potassium cyanide for 20 h. Samples were reduced with dithionite (4 mM) under an atmosphere of Ar, frozen in liquid nitrogen, and measured at 120 K (microwave frequency = 9.47 GHz, modulation amplitude = 1 mT, microwave power = 10 mW). (*C*) Analysis of the Cu in CODH by epr. a, Purified CODH. b, CODH after oxidative wet ashing with sulfuric acid/hydrogen peroxide. c, Protein fraction obtained by ultrafiltration of CODH treated with potassium cyanide. d, Same as c, but after oxidative wet ashing. e, Small molecule fraction obtained by ultrafiltration of CODH treated with potassium cyanide. f, Same as e, but after oxidative wet ashing. Epr spectra were recorded at 50 K (microwave frequency = 9.47 GHz, modulation amplitude = 1 mT, microwave power = 10 mW). (*D*) Stereo view of the [CuSMo(=O)OH] cluster in the active site of CODH. The active site is built up by the bimetallic [CuSMo(=O)OH] cluster in which the two metals are bridged by a μ-sulfido ligand. At the Mo site, the cluster is coordinated by the enedithiolate group of MCD. At the Cu site, the cluster is held by the Sγ of Cys-388. The Mo also carries an apical oxo-group and an equatorial O-atom at a distance of 1.87 Å, which has been modeled as a hydroxo-group, although it is likely that the enzyme in solution carries an oxo-group at this position (11). Glu-763 interacts through its carboxyl atom (Oε2) with the Mo ion in *trans* position to the oxo-group and is linked through hydrogen bonds to the active-site loop carrying Cys-388. Figs. 1*D* and 2 *A–D* were created with BOBSCRIPT (32) and RASTER 3D (33). (*E*) Inactivation of CODH by n-butylisocyanide. (*I*) Effect of the oxidation state of CODH (oxidized, dithionite-reduced, CO-reduced) on the inactivation with 1 mM n-butylisocyanide. (*II*) Specific requirement of the isocyanide group for the inactivation of CODH. The specific CODH activity was determined in the presence of 0.1 μM to 10 mM n-butylisocyanide, n-butanol, or n-butylcyanide, respectively. For experimental details, see *Materials and Methods*.

around 600 nm, which is characteristic of blue Cu-proteins (Fig. 1*A*, trace a; ref. 18).

From data collected at the high-energy side (λ = 0.977 Å) and the low-energy side (λ = 0.980 Å) of the Se-K-absorption edge, anomalous difference Fourier maps were calculated which were the same, particularly at the active site. This result argues against a possible Se at this position.

Anomalous difference Fourier maps calculated from data collected at the high-energy side (λ = 1.378 Å) and the low-energy side (λ = 1.381 Å) of the Cu-K-absorption edge, show the presence of a peak above 9σ only at λ = 1.378 Å at the position formerly assigned to Se. These data identify a Cu at the position where formerly the Se had been modeled. Apparently, the previous interpretation of this anomalous scatterer as Se (7) was mislead because of an inappropriate selection of the low-energy wavelength (λ = 1.732 Å, ref. 7), thereby including the absorption edges of several other elements, including Cu. Although a fluorescence scan showed the presence of Se in CODH crystals, no single Se site could be identified in the anomalous difference Fourier maps. When purified [^{75}Se]-labeled CODH was run on

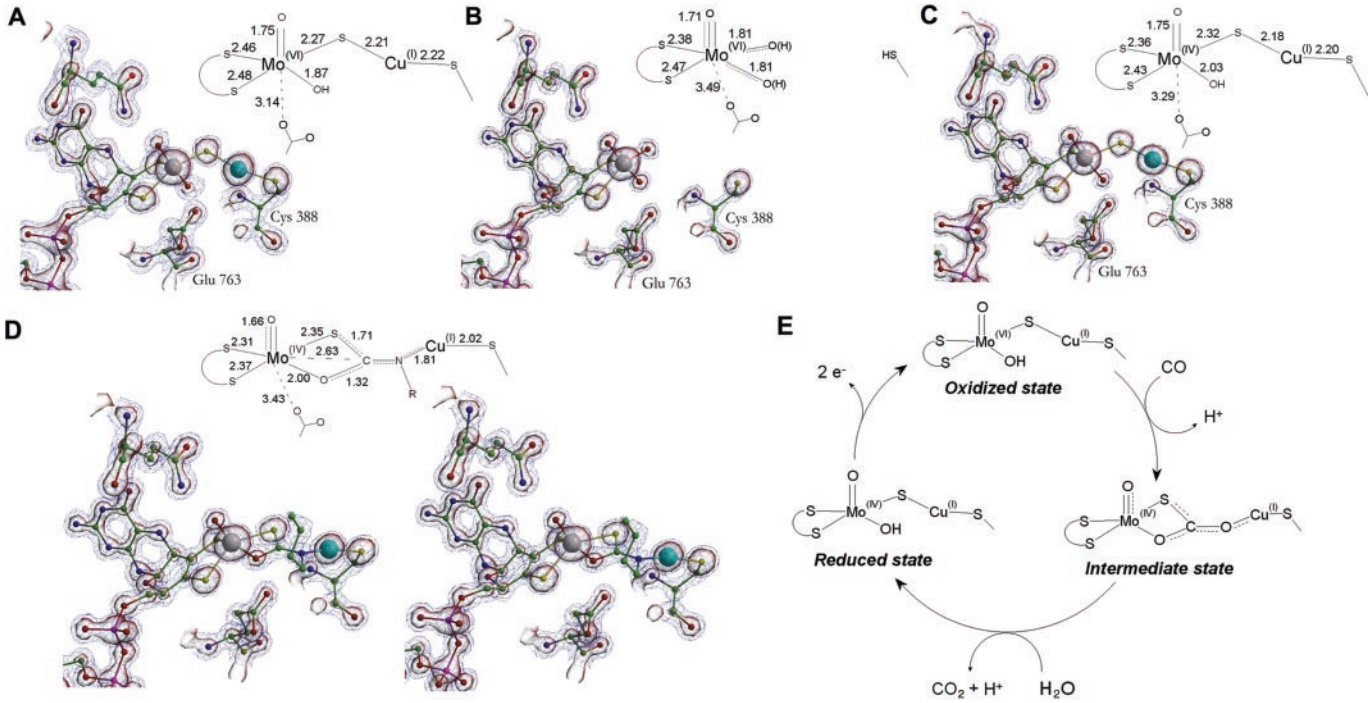

Fig. 2. Geometry of the bimetallic active site at different states. (*A*) The oxidized [CuSMo(═O)OH] site. Additional distances: Cu-Mo, 3.74 Å; hydroxo-Cu, 3.36 Å; Cu-N (Cys-388), 3.14 Å; S8-S7, 3.15 Å; hydroxo-μS, 3.08 Å; hydroxo-Oε2 (Glu-763), 2.99 Å; Mo-Sγ (Cys-388), 5.91 Å. Angles of interest are: hydroxo-Mo-Oxo, 106°; oxo-Mo-μS, 107°; hydroxo-Mo-μS, 96°; Mo-μS-Cu, 113°; μS-Cu-Sγ (Cys-388), 156°; oxo-Mo-S8, 101°; oxo-Mo-S7, 102°; S8-Mo-S7, 79°. (*B*) The cyanide-inactivated [MoO_3] site. Additional distances: hydroxo-hydroxo, 2.71 Å; S8-S7, 3.12 Å; hydroxo-Oε2 (Glu-763), 2.85 Å; Mo-Sγ (Cys-388), 6.61 Å. Angles of interest are: hydroxo-Mo-oxo, 110°; hydroxo-Mo-hydroxo, 97°. (*C*) The reduced [CuSMo(═O)OH] site. The geometry of the reduced site was the same irrespective of whether CO, H_2, or dithionite was used as a reductant. Additional distances: hydroxo-Cu, 3.32 Å; Cu-N (Cys-388), 3.10 Å; S8-S7, 3.14 Å; hydroxo-μS, 2.96 Å; hydroxo-Oε_2 (Glu-763), 2.77 Å; Mo-Sγ (Cys-388), 6.05 Å. Angles of interest are: hydroxo Mo-Oxo, 109°; Oxo-Mo-μS, 107°; hydroxo Mo-S, 86°; Mo-μS-Cu, 122°; μS-Cu-Sγ (Cys-388), 160°; oxo-Mo-S8, 104°; oxo-Mo-S7, 106°; S8-Mo-S7, 82°. (*D*) The n-butylisocyanide-containing site (stereo view). Additional distances: hydroxo-Cu, 3.90 Å; Cu-N (Cys-388), 3.33 Å; S8-S7, 3.08 Å; hydroxo-μS, 2.48 Å; hydroxo-Oε2 (Glu-763), 3.01 Å; Mo-C, 2.63 Å; Mo-Sγ (Cys-388), 6.84 Å; Mo-Cu, 5.07 Å. Angles of interest are: hydroxo-Mo-oxo, 105°; oxo-Mo-μS, 113°; hydroxo-Mo-S, 69°; Mo-μS-Cu, 135°; N (nBIC)-Cu-Sγ (Cys-388), 169°; oxo-Mo-S8, 105°; oxo-Mo-S7, 105°; S8-Mo-S7, 83°. Map coefficients and contour levels are given in parentheses. (σ_A weighted $2F_{obs}-F_{calc}$. Lines at 1.0σ and surface at 2.5σ contoured.) The indicated distances and angles are average values between the two monomers found per asymmetric unit, respectively, in the two high resolution structures in the reduced state. Distances are given in Å. (*E*) Hypothetical scheme showing the oxidation of CO to CO_2 at the [CuSMo(═O)OH] site of CODH. The catalytic cycle starts at the oxidized [CuSMo(═O)OH] cluster with the integration of the CO between the Cu ion and the S- and the equatorial O-ligand of the Mo. The intermediate state shown is hypothetical because its structure has been deduced from the crystal structure of the n-butylisocyanide-bound state (*D*). All other states shown are based on their individual crystal structures (*A* and *C*). In the Transition state, the CO undergoes a nucleophilic attack by the equatorial O with the formation of a thiocarbonate intermediate and reduction of the Mo ion from the +VI to the +IV state. The thiocarbonate then breaks down to CO_2, and the equatorial hydroxo group is regenerated from water, yielding the reduced state of the cluster. Finally, the Mo(+IV) is reoxidized to Mo(+VI) through the transfer of the electrons via FeS I into the intramolecular electron transport, which completes the reaction cycle.

SDS/PAGE and analyzed by autoradiography, the distribution and proportion of label and of methionine residues in the molybdoprotein (61.6% label, 30 residues), the flavoprotein (20.3% label, 9 residues) and the iron-sulfur-protein (18.1% label, 8 residues) were matching. These data suggests that the sulfur of the methionine residues are partially and uniformly replaced by Se during the biosynthesis of CODH in the bacteria.

CODH Contains Sulfur and Copper, Which Are Reactive with Cyanide. Potassium cyanide is known to inhibit the oxidation of CO by CODH (18). Cyanide inactivated the oxidized enzyme with a half-life of 0.5 h (Fig. 1*B*). Complete inactivation resulted in the formation of 1.98 mol of thiocyanate (SCN^-) per mol of enzyme (Fig. 1*B*). In addition, the Cu was completely removed from the enzyme, and upon ultrafiltration, 1.94 mol of Cu per mol of CODH appeared in the small molecule fraction, most likely as CuCN (Fig. 1*B*). Cyanide had no effect on the Mo or Se content of CODH. The inactivation with potassium cyanide changed the characteristic epr spectrum of CODH (Fig. 1*B,* traces a and b). The multiple-line spectrum of the active enzyme (Fig. 1*B*, trace a) disappeared, and a new rhombic signal ($g_1 = 1.977, g_2 = 1.967, g_3 = 1.953, g_{av} = 1.966$) appeared (Fig. 1*B*, trace b). These data indicate that S and/or Cu have an effect on the magnetic state of the Mo ion. The epr spectrum of CODH inactivated by cyanide (Fig. 1*B*, trace b) is very similar to the desulfo-inhibited type of spectra reported for xanthine oxidase/dehydrogenase after abstraction of the cyanolysable sulfur substituent from the Mo (19). These data suggest a sulfur ligand at the Mo ion of CODH.

Architecture of the Oxidized Active Site. The active site of oxidized CODH is built up by an unprecedented dinuclear [CuSMo(═O)OH] metal cluster that is composed of a Cu ion and a Mo-oxo/hydroxo group (Fig. 1*D*). The metals are bridged by a μ-sulfido ligand. The cluster is covalently linked to the large subunit of CODH through interactions of the Cu ion with the Sγ atom of Cys-388, which is part of the unique $VAYRC^{388}SFR$ active-site loop (Fig. 1*D*). The Mo ion is coordinated by the S7′ and S8′ of the molybdopterin cytosine dinucleotide cofactor, which is noncovalently bound to the large subunit (Fig. 1*D*).

The [CuSMo(═O)OH] cluster is, in its composition and geometry, markedly different from any previously observed biological metal cluster or model compound. In fact, the occurrence of Mo in a dinuclear heterometal cluster is completely

unexpected, as all known molybdopterin-containing or molybdopterin dinucleotide-containing molybdoenzymes are mononuclear (20). In addition, the [CuSMo(=O)OH] cluster is unrelated to the $[S_2MoS_2CuS_2MoS_2]^{3-}$ mixed metal-sulfide cluster of the orange protein from *Desulfovibrio gigas* (21).

The ligands around Mo form a distorted square pyramidal geometry (Figs. 1*D* and 2*A*). The dithiolate group of MCD is positioned in the equatorial plane together with one O and one S group, which were modeled as a hydroxo- and a sulfido-group. The apical ligand was modeled as an oxo-group. Residues in the second coordination sphere around the Mo are Gln-240 and Glu-763 (Fig. 1*D*). The Nε2 group of Gln-240 is with 2.90 Å in hydrogen-bonding distance to the apical oxo-ligand at the Mo ion. Oε2 of Glu-763 and N of Ser-389 (2.60 Å), as well as Oε1 of Glu-763 and Oγ of Ser-389 (2.80 Å), are in hydrogen-bonding distances (Fig. 1*D*). Oε2 of Glu-763 is also in hydrogen-bonding distance to the equatorial hydroxo-ligand (3.0 Å) and donates a negative charge in a distance of 3.14 Å to the Mo ion (Fig. 2*A*). These hydrogen bonds remain essentially the same in CODH oxidized with air (Fig. 2*A*), inactivated with cyanide (Fig. 2*B*), reduced with CO (Fig. 2*C*), or treated with n-butylisocyanide (Fig. 2*D*).

The μ-sulfido ligand and the Sγ atom of Cys-388 ligate the Cu ion in a distorted linear geometry (Fig. 1*D*). A two-coordinate linear geometry is found in several Cu(+I) complexes (22), and the model compound $[Cu(SC_{10}H_{13})_2]^-$ shows the same type of ligands and coordination with Cu…S distances of 2.137 Å and a S-Cu-S angle of 178.6° (23), indicating a +I oxidation state of the Cu in the active site of CODH. This is also in agreement with a diamagnetic epr spectrum obtained under appropriate conditions (Fig. 1*C*, trace a) and the generation of a paramagnetic Cu(+II) signal ($g_{\|} = 2.396$, $g_{\perp} = 2.081$, $A_{\|} = 13.3$ mT) which appeared upon oxidative wet ashing of CODH (Fig. 1*C*, trace b).

Cyanide-Inactivated Active-Site Structure. When crystals of air-oxidized CODH were soaked with aqueous potassium cyanide, the Cu ion and the μ-sulfido ligand were removed from the bimetallic cluster (Fig. 2*A*) and a mononuclear Mo cluster with three O ligands remained (Fig. 2*B*). Epr indicates that Cu(+I) is released upon treatment of CODH with cyanide (Fig. 1*C*, trace e) which can be oxidized to Cu(+II) (Fig. 1*C*, trace f). Near the former position of the μ-sulfido ligand, an additional hydroxo/oxo-ligand now completes the coordination of the Mo ion. The two equatorial O ligands have the same bond lengths as Mo, with values between the typical bond length of oxo- and hydroxo-ligands (Fig. 2*B*). In cyanide-inactivated CODH, the Sγ-atom of Cys-388 has moved away from the Mo ion by 0.7 Å (Fig. 2*B*), compared with the oxidized enzyme (Fig. 2*A*). Apparently, the interaction of the Sγ atom with the Cu establishes a tensed conformational state of the oxidized [CuSMo(=O)OH] cluster (Figs. 1*D* and 2*A*).

Reduced Active-Site Structure. Because the bimetallic cluster participates in redox-catalysis, we were interested to examine its structure in the reduced form. Reduction of CODH by CO, H_2, or sodium dithionite under anoxic conditions in solution (Fig. 1*A*) or in crystals is accompanied by a color change from dark brown to faint green. We collected datasets of crystals, which have been completely reduced before shock freezing. The refined structures of reduced CODH were indistinguishable and showed the same active-site geometry, irrespective of whether CO, H_2, or dithionite were used as reductants (Fig. 2*C*). Reduction of air-oxidized CODH results in an increase of the Cu…Mo distance from 3.74 to 3.93 Å and of the Mo…OH distance from 1.87 to 2.03 Å (Fig. 2*A* and *C*). The corresponding distances determined by EXAFS were 3.70 and 4.23 Å or 1.74 and 2.16 Å, respectively (11). We assume that the disagreement in distances observed by crystallography and EXAFS can be attributed to the different physicochemical states of the samples (crystals and solutions, respectively). The reduced cluster shows an increased distance between the Mo and the carboxyl-group of Glu-763, along with slightly decreased Mo-S dithiolate bond lengths (Fig. 2 *A* and *C*). Bound substrate (CO) or reductant (dithionite) were not observed at the active site. The conformation of the pterin moiety of the MCD cofactor was the same in oxidized and reduced CODH.

N-Butylisocyanide-Bound Active-Site Structure. Carbon monoxide (|C≡O|) and the isocyanide group (|C≡N-R) show similar reactivities because they are isoelectronic, display a similar σ-donor and π-acceptor ligand character, and share the presence of a nonbonding pair of electrons in the *sp*-hybridized orbital of the terminal carbon atom. Indeed, n-butylisocyanide (Fig. 1*E*) or benzylisocyanide (not shown) act as inhibitors of oxidized CODH, whereas the reduced enzyme was not affected (Fig. 1*E*). CODH inhibited with n-butylisocyanide was Mo-epr silent in the temperature range from 16 to 120 K. After reductive titration with dithionite, a weak "desulfo"-signal appeared, which could be attributed by spin integration to 7% of the total Mo.

In the n-butylisocyanide-inhibited CODH, the Cu ion was also epr silent from 16 to 120 K. These data suggest the oxidation states +IV and +I for Mo and Cu, respectively. Supporting evidence for these oxidation states comes from the positions and shapes of the Mo- and Cu-K-edges of inactivated CODH revealed by XAS (M. Gnida, L.G., W. Meyer-Klaucke, and O.M., unpublished results).

Datasets were obtained from crystals soaked with 10 mM n-butylisocyanide for 2 h. The crystal structure shows the isocyanide group at the [CuSMo(=O)OH] cluster, forming covalent bonds to the μ-sulfido ligand, the hydroxo ligand and the Cu atom (Fig. 2*D*). The alkyl chain of the n-butylisocyanide extends into the hydrophobic interior of the substrate channel. The structure formed between Mo and Cu is equivalent to a thiocarbamate derivative in which the oxygen and sulfur are the Mo ligands and the carbon and nitrogen originate from the isocyanide. The resulting planar four-membered metallocycle at the Mo ion exhibited short distances between nonbonded ring members (Fig. 2*D*), with a distance of 2.63 Å between the C-atom of n-butylisocyanide and Mo and of 2.48 Å between the sulfur and the oxygen. Binding of the isocyanide caused larger structural changes for all atoms of the [CuSMo(=O)OH] cluster, resulting in an "open state," in which the distance between Cu and Mo increased from 3.74 to 5.07 Å. Additionally, the opening of the cluster resulted in an increase of the distance between Oε2 of Glu-763 and Mo by 0.3 Å (Fig. 2 *A* and *D*). A stronger interaction between Mo and its formerly double-bonded oxo-ligand completes the observed changes for all ligands at Mo and Cu (Fig. 2 *A* and *D*).

After the ligand substitution, the Cu is ligated in a linear coordination by the N atom of n-butylisocyanide and, as before, by the Sγ atom of Cys-388 (Fig. 2*D*). The bond lengths for the two Cu ligands shown in Fig. 2*D* are somewhat shorter than expected for single bonds at Cu, which are 1.92 Å (Cu-N) or 2.14 Å (Cu-S; refs. 22 and 23). The observed bond length shortening can be explained by assuming a donation of electrons from Cu to the N atom of n-butylisocyanide, which is compensated for by the Cu-S bond.

Discussion

CO Oxidation at the [CuSMo(=O)OH] Cluster. By analogy with the thiocarbamate derivative formed through the reaction of n-butylisocyanide with the bimetallic cluster of CODH (Fig. 2*D*), a thiocarbonate intermediate state is proposed for the oxidation of CO (Fig. 2*E*, Intermediate state). According to the model depicted in Fig. 2*E*, CO is inserted between the Cu, the sulfido-ligand and the equatorial hydroxo-group of the bimetal-

lic cluster. The ligand substitution at the Cu is presumably reinforced by relaxing the tensed state of the oxidized cluster through the retraction of Cys-388. In the thiocarbonate intermediate state, the Cu moves away from the Mo, thereby giving rise to the "open state" of the cluster (Fig. 2*E*, Intermediate state). A likely function of the Oε2 of Glu-763 is the stabilization of the Mo(+VI) state (Figs. 1*D* and 2*A*). Therefore, the increase of the Mo…Oε2 distance, as apparent from the n-butylisocyanide-bound state (Fig. 2*D*), might destabilize the Mo(+VI) and initiate its reduction. The proximity of the sulfido ligand to Mo(+VI) suggests a noninnocent role of the ligand in Mo(+VI) reduction involving an internal electron transfer (24) effected by the binding of CO between Cu(+I) and the sulfido ligand. The insertion of CO results in an increased electrophilicity of its carbon atom which allows its reaction with the nucleophilic equatorial hydroxo-group at the Mo. The reaction also might be driven by the increased bond order of the oxo-group (25), as observed in the n-butylisocyanide bound form (Fig. 2*D*). The supplied energy is believed to stabilize the thiocarbonate intermediate state in which the formal oxidation of the CO carbon from (+II) to (+IV) has already occurred (Fig. 2*E*, Intermediate state). The formation of CO_2 from the thiocarbonate intermediate is presumably driven by the stability of the product. According to the model, product formation and release occur cooperatively with closure of the cluster and replacement of the incorporated hydroxo ligand by water (Fig. 2*E*). The Mo-O bond length in the CO-reduced cluster is much shorter than expected for a water ligand (Fig. 2*C*) and indicates a hydroxo group and the requirement for an initial deprotonation with the possible assistance of Glu-763 (Fig. 2*E*, Reduced state).

The oxidation of H_2 by CODH was inhibited by n-butylisocyanide as well, suggesting that it occurs at the metal cluster. The known promotion of the heterolytic cleavage of H_2 by Cu(+I) salts (26) suggests a function of the cuprous ion in the oxidation of H_2. The alternation between closed (Fig. 2*E*, Oxidized and Reduced state) and opened state (Fig. 2*E*, Intermediate state) of the cluster would allow for the binding and cleavage of H_2, with an intermediate hydride ion bound to Cu(+I).

Mono- and Dinuclear Mo-Containing Enzymes. The structural characterization of the [CuSMo(=O)OH] cluster at different states revealed some of the versatile possibilities that the element quartet Mo, S, O, and Cu are offering for catalysis in nature. All metals and ligands of the cluster have been found to fulfill crucial catalytic tasks. Up to now, Mo was known in biological systems as an integral component of the multinuclear center of nitrogenases and the active site of the mononuclear Mo-enzymes, such as xanthine oxidase, sulfite oxidase, and DMSO reductase (20). The dinuclear [CuSMo(=O)OH] site of the CODH from the aerobic eubacterium *O. carboxidovorans* is a third basic form of Mo in active biological systems and establishes the class of the dinuclear molybdoenzymes containing the pterin cofactor. Although the function of the [CuSMo(=O)OH] cluster in CODH is the oxidation of CO, the Mo environment and the quaternary structure are also conserved in the mononuclear Mo hydroxylases (27–29), suggesting that the catalytic roles of the Mo environment in CODH also apply to them. The remarkable and previously uncharacterized role of Cu in allowing ligand insertion and substitution through changes between the opened and closed state of the cluster, thereby altering the direct Mo environment, is not known of other molybdoenzymes and is entirely different from other characterized mono- or polynuclear Cu-containing enzymes (30).

We thank G. B. Bourenkov (BW6, Deutsches Elektronen Synchrotron, Hamburg, Germany) for his help in data collection and multiple wavelength anomalous dispersion measurements. This work was supported by European Union Grant IHP-RTN-99-1 (to H.D. and R.H.) and by Deutsche Forschungsgemeinschaft, Bonn, Grant Me 732/8-1 (to O.M.).

1. Moersdorf, G., Frunzke, K., Gadkari, D. & Meyer, O. (1992) *Biodegradation* **3,** 61–82.
2. Ragsdale, S. W. & Kumar, M. (1996) *Chem. Rev. (Washington, D.C.)* **96,** 2515–2539.
3. Fontecilla-Camps, J. C. & Ragsdale, S. W. (1999) in *Advances in Inorganic Chemistry*, eds. Sykes, A. G. & Cammack, R. (Academic, London), Vol. 47, pp. 283–333.
4. Svetlitchnyi, V., Peschel, C., Acker, G. & Meyer, O. (2001) *J. Bacteriol.* **183,** 5134–5144.
5. Dobbek, H., Svetlitchnyi, V., Gremer, L., Huber, R. & Meyer, O. (2001) *Science* **293,** 1281–1285.
6. Drennan, C. L., Heo, J., Sintchak, M. D., Schreiter, E. & Ludden, P. W. (2001) *Proc. Natl. Acad. Sci. USA* **98,** 11973–11978.
7. Dobbek, H., Gremer, L., Meyer, O. & Huber, R. (1999) *Proc. Natl. Acad. Sci. USA* **96,** 8884–8889.
8. Meyer, O., Gremer, L., Ferner, R., Ferner, M., Dobbek, H., Gnida, M., Meyer-Klaucke, W. & Huber, R. (2000) *Biol. Chem.* **381,** 865–876.
9. Gremer, L., Kellner, S., Dobbek, H., Huber, R. & Meyer, O. (2000) *J. Biol. Chem.* **275,** 1864–1872.
10. Hänzelmann, P., Dobbek, H., Gremer, L., Huber, R. & Meyer, O. (2000) *J. Mol. Biol.* **301,** 1221–1235.
11. Gnida, M., Ferner, R., Gremer, L., Meyer, O. & Meyer-Klaucke, W. (2002) *Biochemistry*, in press.
12. Kraut, M., Hugendieck, I., Herwig, S. & Meyer, O. (1989) *Arch. Microbiol.* **152,** 335–341.
13. Kiefersauer, R., Than, M. E., Dobbek, H., Gremer, L., Melero, M., Strobl, S., Dias, J. M., Soulimane, T. & Huber, R. (2000) *J. Appl. Crystallogr.* **33,** 1223–1230.
14. Sheldrick, G. M. & Schneider, T. R. (1997) *Methods Enzymol.* **277,** 319–343.
15. Murshudov, G. N., Lebedev, A., Vagin, A. A., Wilson, K. S. & Dodson, E. J. (1999) *Acta Crystallogr. D* **55,** 247–255.
16. McRee, D. (1993) *Practical Protein Crystallography* (Academic, New York).
17. Turk, D. (1992) Ph.D. thesis (Technische Universität München, Germany).
18. Meyer, O. (1982) *J. Biol. Chem.* **257,** 1333–1341.
19. Bray, R. C. (1975) in *The Enzymes*, ed. Boyer, E. D. (Academic, New York), Vol. 12, pp. 300–419.
20. Hille, R. (1996) *Chem. Rev.* **96,** 2757–2816.
21. George, G. N., Pickering, I., Yu, E. Y., Prince, R. C., Bursakov, S. A., Gavel, O. Y., Moura, I. & Moura, J. J. G. (2000) *J. Am. Chem. Soc.* **122,** 8321–8322.
22. Hathaway, B. J. (1987) in *Comprehensive Coordination Chemistry* (Pergamon, Oxford), pp. 533–774.
23. Koch, S. A., Fikar, R., Millar, M. & O'Sullivan, T. (1984) *Inorganic Chemistry* **23,** 121–122.
24. Stiefel, E. I. (1997) *J. Chem. Soc. Dalton Trans.* **21,** 3915–3923.
25. Rappe, A. K. & Goddard, W. A., III (1980) *Nature* **285,** 311–312.
26. Pasquali, M. & Floriani, C. (1983) in *Copper Coordination Chemistry: Biochemical and Inorganic Perspectives*, eds. Karlin, K. D. & Zubieta, J. (Adenine, Guilderland, NY), pp. 311–330.
27. Romao, M. J., Archer, M., Moura, I., Moura, J. J., LeGall, J., Engh, R., Schneider, M., Hof, P. & Huber, R. (1995) *Science* **270,** 1170–1176.
28. Enroth, C., Eger, B. T., Okamoto, K., Nishino, T., Nishino, T. & Pai, E. F. (2000) *Proc. Natl. Acad. Sci. USA* **97,** 10723–10728.
29. Truglio, J. J., Theis, K., Leimkühler, S., Rappa, R., Rajagopalan, K. V. & Kisker, C. (2002) *Structure (London)* **10,** 115–125.
30. Messerschmidt, A. (1998) in *Comprehensive Biological Catalysis* (Academic, New York).
31. Westley, J. (1981) *Methods Enzymol.* **77,** 285–291.
32. Esnouf, R. M. (1997) *J. Mol. Graphics* **15,** 132–134.
33. Merritt, E. A. & Bacon, D. J. (1997) *Methods Enzymol.* **277,** 505–524.